Compositional and structural studies of ion-beam modified AlN/TiN multilayers

M. Amati[a,*], Luca Gregoratti[a], H. Sezen[a], A. Grce[b], M. Milosavljević[b], K.P. Homewood[c]
[a]*Elettra - Sincrotrone Trieste SCpA, Area Science Park, 34149 Trieste, Italy*
[b]*VINČA Institute of Nuclear Sciences, Belgrade University, P.O. Box 522, 11001 Belgrade, Serbia*
[c]*Materials Research Institute and School of Physics and Astronomy, Queen Mary University of London, Mile End Road, E1 4NS, London, United Kingdom*

Abstract

This paper reports on compositional and structural modifications induced in coated AlN/TiN multilayers by argon ion irradiation. The initial structure consisting of totally 30 alternate AlN (8 nm thick) and TiN (9.3 nm thick) layers was deposited on Si (100) wafers, by reactive sputtering. Irradiation was done with 180 keV Ar^+ to a high dose of $8x10^{16}$ ions/cm^2, which introduces up to ~8 at.% of argon species, and generates a maximum displacement per atom of 92 for AlN and 127 for TiN, around the projected ion range (109±34 nm). Characterizations were performed by Rutherford backscattering spectrometry, spatially resolved x-ray photoelectron spectroscopy, and transmission electron microscopy. The obtained results reveal that this highly immiscible and thermally stable system suffered a severe modification upon the applied ion irradiation, although it was performed at room temperature. They illustrate a thorough inter-layer mixing, atomic redistribution, structural change and phase transformation within the affected depth. The original TiN layers appear to grow in thickness, consuming the adjacent AlN layers, while retaining the fcc crystalline structure. In the mostly affected region, the interaction proceeds until all of the original AlN layers are consumed. Compositional studies with photoemission spectroscopy show that due to the ion irradiation treatment the TiN and AlN layers are transformed into $Ti_{0.75}Al_{0.25}N$ and $Ti_{0.65}Al_{0.35}N$ ternary compounds characterized by a better homogenized chemical form compared to non-irradiated layers. The results can be interesting towards further development of radiation tolerant materials based on immiscible ceramic nanocomposites.

Keyword

Interlayer; mixing; SPEM; radiation tolerant; phase transformation.

1. Introduction

High strength composites of nano-scaled immiscible multilayers are potentially interesting as radiation tolerant materials [1-3]. The contribution of multiple interfaces is in enhancing the mechanical

strength of the structure, as well as in enabling fast diffusion paths for trapping and releasing of radiation induced point defects. Furthermore, mutual immiscibility of components suppresses inter-layer mixing, which can be significant at high irradiation doses, and can lead to degradation of the multilayered structure. Ion irradiation tolerance was demonstrated on a number of immiscible metallic multilayered systems, such as Cu/Nb, Cu/W, Ag/Ni, or Ta/Ti [2-6]. Recent developments report a novel approach for fabricating a 4 mm-thick Cu/Nb multilayered crystallographically stable nanocomposite via accumulative roll bonding technique [7], opening a significant route for bulk nanocomposites as structural materials in advanced nuclear power systems. Another class of potentially interesting materials are nanolayered ceramics, such as AlN/TiN or CrN/TiAlN [8-11]. In general, ceramics are resistant to radiation induced amorphization and swelling [12], and in a multilayered form the components are typically immiscible.

This work reports a study of structural and compositional changes induced upon high dose argon ion irradiation of AlN/TiN multilayers. The immiscible AlN/TiN multilayered system is known to exhibit high mechanical strength, good corrosion resistance, and thermodynamic stability up to 1000 ^{o}C, due to a large positive value of reaction enthalpy. However, a previous report has demonstrated that high argon ion doses (4-8x10^{16} ions/cm^2) induce a considerable inter-layer mixing if such structure is composed of very thin (<10 nm) layers, although irradiation was performed at room temperature [13]. Such behavior was assigned to a high rate of atomic collisions, which generate a large amount of knock-ons that cross over the interfaces, and could not be compensated by the opposing chemical driving forces in this immiscible system. The aim of this work was an in-depth study of the compositional changes and phase transformation in case of this heavily intermixed AlN/TiN structure. The focus was on high sensitivity spatially resolved scanning photoelectron microscopy (SPEM) and microprobe x-ray photoelectron spectroscopy (XPS) studies at the boundaries of non-irradiated and irradiated areas, for which a special sample preparation technique with a grazingly polishing procedure is introduced (see the supplementary material).

2. Characterization technique

Compositional and structural characterizations of samples were performed by Rutherford backscattering spectrometry (RBS), spatially resolved x-ray scanning photoelectron microscopy (SPEM), transmission electron microscopy (TEM), and atomic force microscopy (AFM)

2.1 Rutherford backscattering spectrometry (RBS)

RBS was done with 1.029 and 1.534 MeV He^+ ion incident beam, random spectra were collected at normal incidence and 45° tilt, with two detectors positioned at 149° and 172° scattering angles, the data were analyzed as described previously.

2.2 Scanning photoelectron microscopy (SPEM)

SPEM experiments were performed at the ESCAmicroscopy beamline at the Elettra synchrotron radiation facility located in Trieste, Italy. Synchrotron source x-ray beam is focused on the sample with a diameter of around 150 nm using Fresnel zone plate optics. In SPEM the sample can be raster scanned with respect to the microprobe [14]. Photoelectrons are collected, energetically resolved with an electron hemispherical analyzer (HEA) and detected by a 48-channels electron detector. The position of the HEA with respect to the sample surface is fixed at 30 degrees. This configuration strongly enhances the surface sensitivity of the instrument. SPEM can be operated in two modes: (i) imaging spectromicroscopy and (ii) microspot spectroscopy. The imaging mode maps the lateral distribution of elements by collecting photoelectrons with a selected kinetic energy window while scanning the specimen with respect to the microprobe. When the element under consideration is present in a single chemical state, the spatial variation in the contrast of the images reflects the variation of the photoelectron yield, which is a measure of the local concentration of the element. The images were recorded with fixed kinetic energy windows corresponding to the peak positions of Ti $2p_{3/2}$, Al 2p, and N 1s. The microspot mode is identical to the conventional x-ray photoelectron spectroscopy (XPS), i.e. energy distribution curves are measured from the illuminated local micro-spot area. Spatially resolved photoemission spectra of selected regions and chemical maps were acquired with 0.2 eV overall energy resolution by using 655 eV photon energy. For a renormalization procedure to calculate Ti and Al concentrations for ternary compounds from the line-shapes of Ti $2p_{3/2}$ core-line in literature works, acquired with a 1486.7 eV x-ray beams, the cross-sections and attenuation lengths are obtained from the NIST database [15].

2.3 Transmission electron microscopy (TEM)

TEM analysis was done on a Jeol JEM-200 electron microscope operated at 200 kV. For these characterization samples were prepared for cross-sectional analysis by ion-beam thinning. Selected area electron diffraction (SAED) patterns were analyzed using the ELD software [16].

2.4 Atomic force microscopy (AFM)

AFM experiments have been performed with a XE-100 Park Instruments, in contact mode using commercial silicon tips (CSC38 Mikromasch, spring constant=0.03-0.09 N/m). Topographic images have been acquired with a scan size ranging from 10 to 40 micrometers and 256/512 pixel resolution. Raw data has been analyzed using Gwyddion software to extract roughness and line profiles.

3. Sample preparation

The investigated AlN/TiN multilayered structures were prepared by reactive sputter deposition, from 99.9 % Al and Ti targets, using Si (100) wafers as substrates, held at ambient temperature during deposition. The structures consisted of 30 alternate AlN (8 nm thick) and TiN (9.3 nm thick) layers, with a total thickness of 260 nm. The first layer deposited on Si-substrate was TiN, and the outermost AlN. Ion irradiation was performed at normal incidence with singly charged Ar ions, at 180 keV, to a dose of 8×10^{16} ions/cm^2, over a uniformly scanned sample area of 2.5×2.5 cm. The targets were mounted on a water-cooled sample holder, and the ion current was maintained at ~1 μA/cm^2 to avoid beam heating. The method of stopping and range of ions in solids (SRIM) [12], evaluations give the projected ion range of $Rp\pm\Delta Rp=109\pm34$ nm, a maximum around 8 at.% of implanted Ar in the structure, a maximum displacements per atom (*dpa*) of 92 for AlN and 127 for TiN, and predict up to 20% Al-Ti intermixing due to atomic collision cascades (not considering the role of repelling chemical driving forces) as shown Fig. 1.

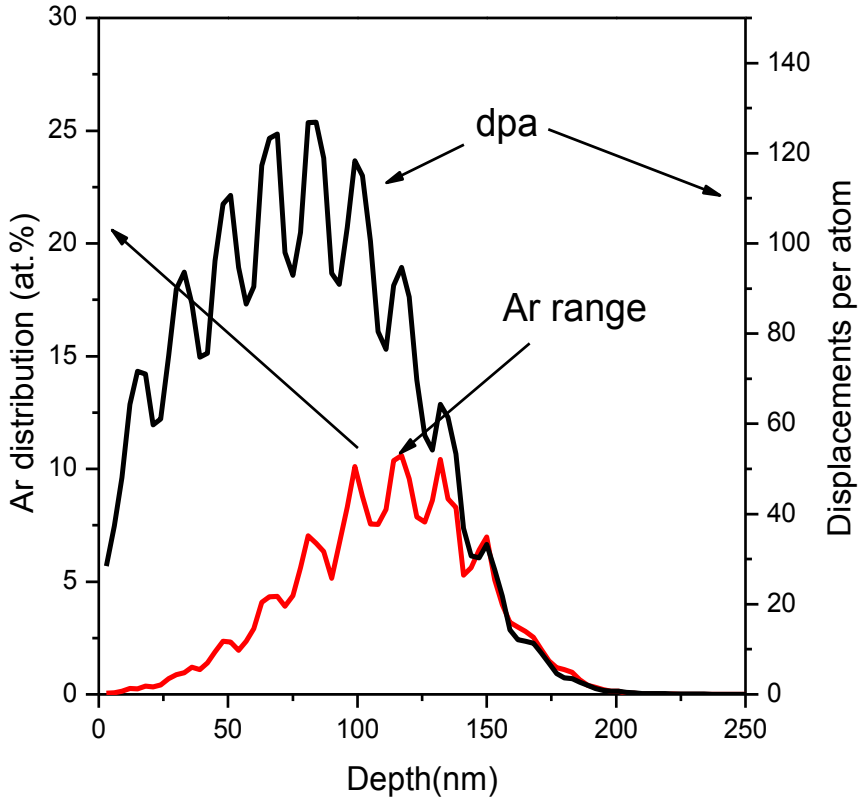

Fig. 1. Ar distribution and displacements per atom (*dpa)* evaluated by SRIM

A special preparation of samples was needed in order to make the buried AlN and TiN thin layers visible to XPS which is a surface sensitive technique where the in depth analysis is limited, in the case of SPEM, up to the few outermost atomic layers. The multilayered TiN/AlN sample was polished at a grazing angle. The set of proper parameters for the polishing procedure of samples, e.g. grazing angle used for lapping, lapping powder/speed and time, etc., have been regulated to bring the buried TiN and AlN layers to the surface with large enough dimensions.

Investigations have been done with grazingly-lapped multilayered TiN/AlN sample around a border of highly irradiated and non-irradiated zones.

The presence of the unconcealed buried layers is confirmed by both AFM and SPEM image. The AFM image in Fig. 2(a) shows the appearance of a number of layers after the lapping procedure which are comparable with elemental SPEM images in Fig. 2(a), and each of them was exposed in the surface for few hundreds of μm. In order to prove that each band represents the correct sequence of layers we measured the height profile across consecutive boundaries. A typical profile shown in Fig. 2(b) illustrates the heights corresponding to the nominal thickness of the TiN and AlN layers.

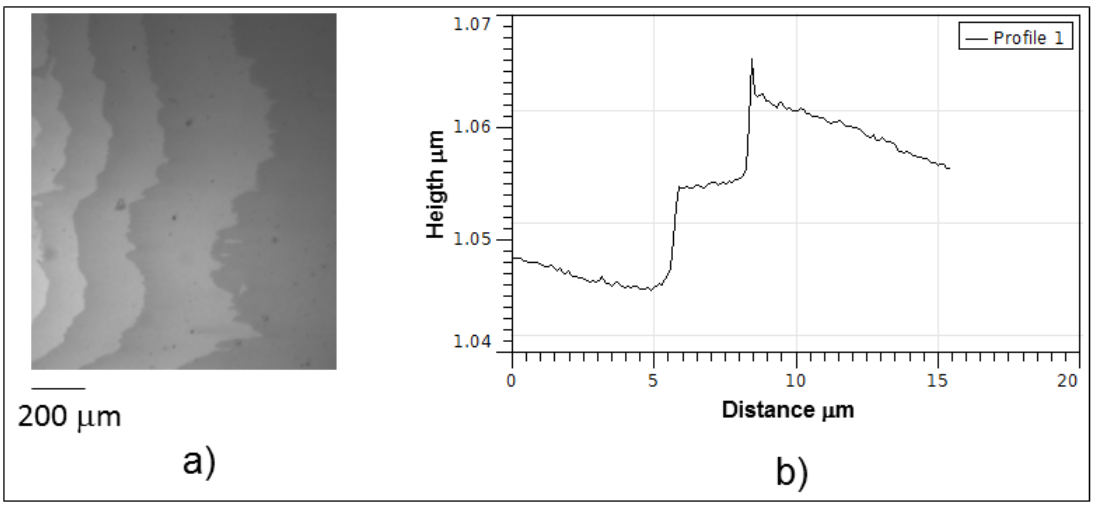

Fig. 2. (a) 1.2x1.0 mm2 optical image from a grazingly lapped multilayered TiN/AlN sample.(b) a typical AFM profile across the lapped surface showing the nominal thickness of the layers.

The elemental Ti and Al profiles obtained from SPEM images are shown in Fig. 3.

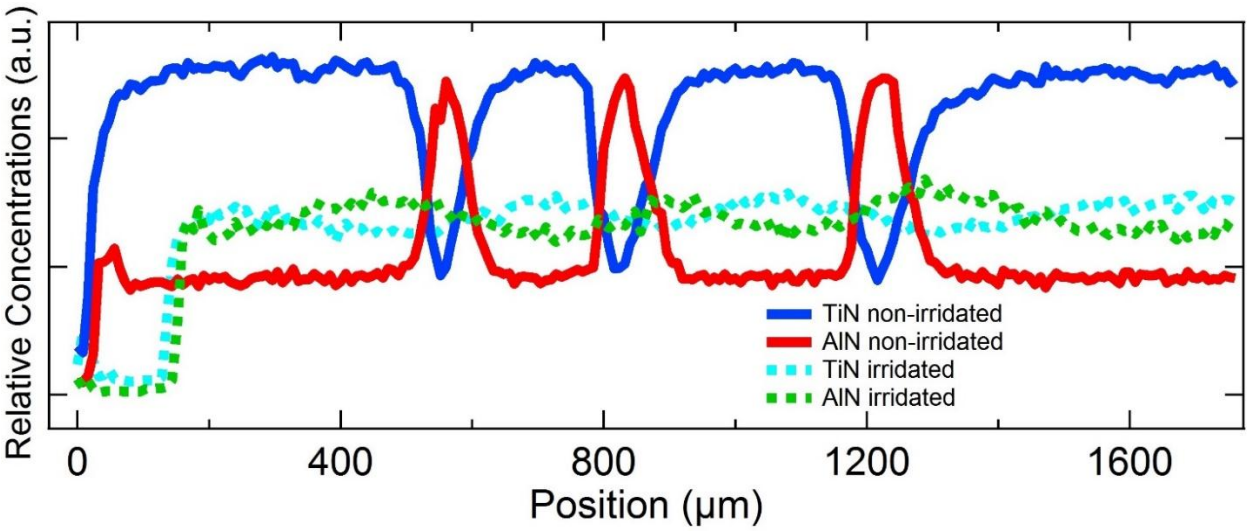

Fig. 3. Ti and Al elemental profiles extracted from corresponding regions of the SPEM images in Fig. 5(a).

4. Results and discussion

Experimental Rutherford backscattering spectrometry (RBS) spectra taken from non-irradiated and irradiated samples, at normal incidence, with 1.534 MeV He^+ ion-beam, are shown in Fig. 4(a). Surface positions of Ti, Al and N signals are indicated by vertical arrows. The Ti surface signal is shifted to lower energies, by ~30 keV, as the first on top layer is AlN. The position of surface Al coincides with

the low energy edge of Ti distribution, and the signal stretches to the Si-substrate. Nitrogen distribution is superimposed on top of the signal arising from the Si-substrate. The presence of light element impurities, such as C or O was below the detection limit of the system. By comparing the two spectra, it can be concluded that ion irradiation induces an increase in depth of the multilayered AlN/TiN structure, which can be seen from the increase in the width of both Ti and N signals. The multilayered nature of the structure is barely observed from irregular shape of the signals. Implanted Ar is buried into the structure, approximately around the projected ion range deduced by a method of the stopping and range of ions in solids (SRIM). The Ar signal is overlapped by the signal arising from Ti. To illustrate this point a separated Ar spectrum deduced by fitting the experimental data is put as an inset at the bottom of the plot (blue line).

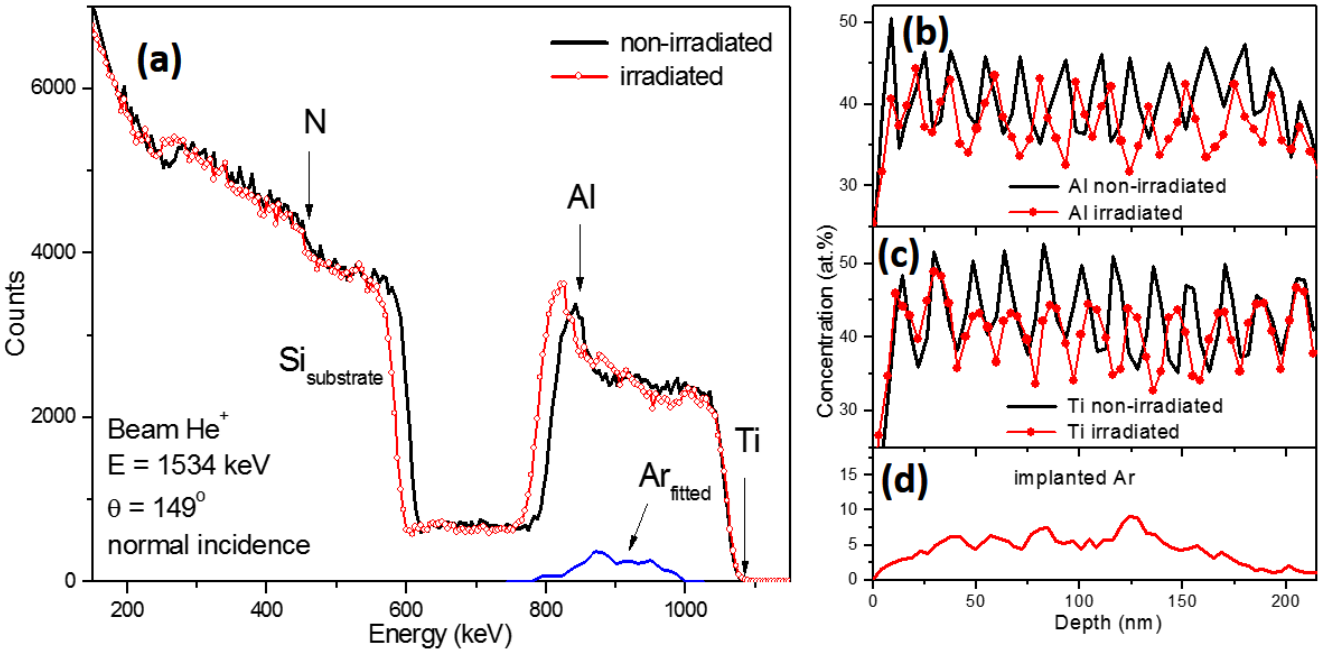

Fig. 4. (a) RBS spectra have been taken from non-irradiated and irradiated samples, at normal incidence. Inset is a fitted Ar signal obtained by analyzing the data of the irradiated sample. Extracted Al (b), Ti (c) and Ar (d) depth profiles of non-irradiated and irradiated samples.

Better depth resolution analysis of the surface layers was accomplished by reducing the He^+ energy to 1.025 MeV and tilting the samples to 45° off normal incidence. Extracted Al, Ti and Ar depth profiles from the RBS spectra taken from non-irradiated and irradiated samples are shown in Fig. 4(b-d). Nitrogen depth distribution is omitted for clarity. The analysis suggests that before irradiation the TiN layers are stoichiometric (Ti:N ~ 50:50), while the AlN layers are slightly under-stoichiometric (Al:N ~ 45:55). The depth range presented in Fig. 4(b,c) covers approximately the top 12 AlN/TiN bilayers,

where most of the implanted Ar is distributed. Upon ion irradiation, the Al and Ti peaks become lower and wider, which is especially expressed in Ti distribution. For instance, the same depth covered by 12 AlN/TiN bilayers in non-irradiated sample is covered by 11 bilayers in the irradiated sample. The Al and Ti concentration reduces mostly in the regions where these species are substituted by the implanted Ar and atomic intermixing occurs. Argon is distributed throughout the presented depth range, with a maximum of ~8 at.% at a depth of ~125 nm (see Fig. 1), which is in a fair agreement with the predictions calculated by the SRIM software suite [12].

A similar investigation has been done with the grazingly-lapped multilayered TiN/AlN sample around a border of highly irradiated and non-irradiated zones. The adventitious carbon and overlayered oxides were properly cleaned by a mild low energy sputtering treatment of sample surface which was verified by XPS not altering the surface chemistry and stoichiometry of sample. As illustrated in Fig. 5(a) the two elemental photoelectron images clearly demonstrate alternated TiN and AlN layers spanning horizontally in the multilayered TiN/AlN sample, and a distinct vertical border separates the non-irradiated (left side) and irradiated (right side) zones from each other. The appearance of TiN and AlN layers on SPEM images are equally comparable with the AFM image, see Fig. 2. In the non-irradiated section TiN layers have broader widths than AlN layers. The possible reason of this difference raises probably from the characteristic material properties of TiN and AlN layers. Namely, the AlN material is softer than TiN one, so it is more easily raptured during the polishing resulting in a much smaller opened surface area for AlN layers than TiN layers. The elemental contrast between TiN and AlN layers is clearer and sharper in the non-irradiated side, but, as expected, in the irradiated region the widths of both TiN and AlN layers extend, and the boarders between consecutive TiN and AlN layers become fainter due to atomic intermixing. In addition, the horizontally spanning of TiN and AlN layers are remarkably bending when they are approaching the border between the irradiated and non-irradiated zones. The possible reason could be an increase of thickness at the irradiated part due to Ar implantation.

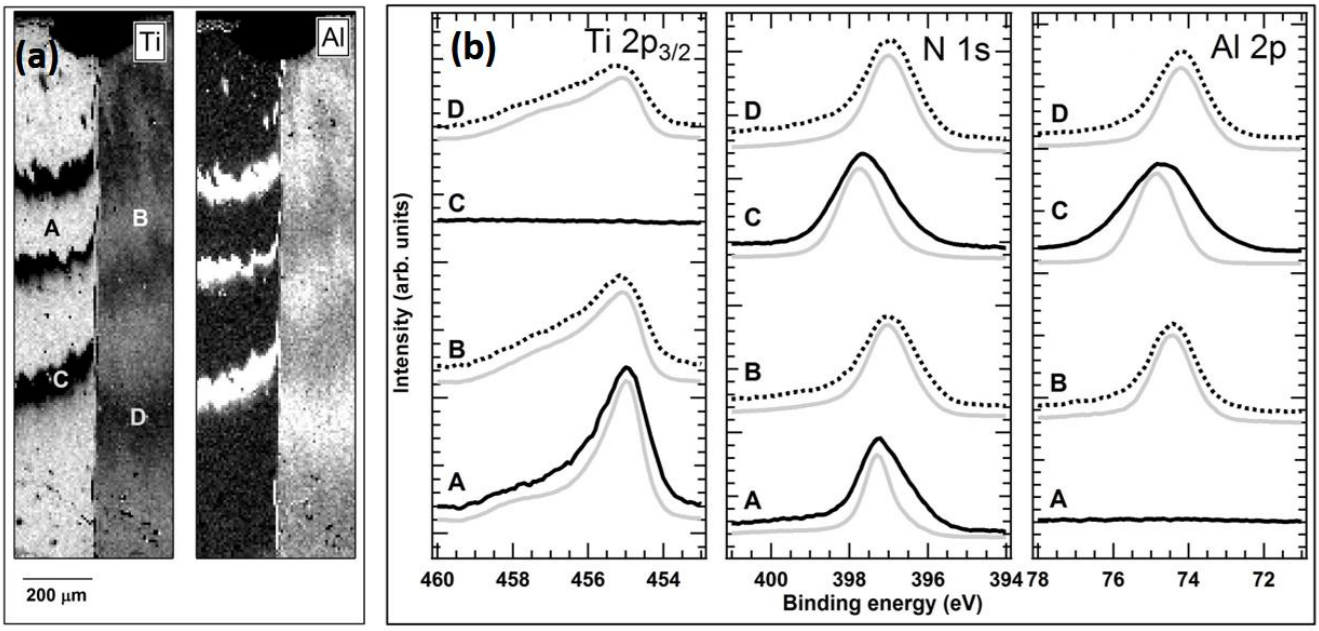

FIG. 5. (a) Ti $2p_{3/2}$, and Al 2p maps of the irradiated and non-irradiated multilayered TiN/AlN sample. The labels, A-D, on the Ti image indicate where microprobe spectra have been collected. (b) Ti $2p_{3/2}$, N 1s and Al 2p core level spectra acquired on non-irradiated TiN (label A, solid lines) and AlN (label C, solid lines) layers and irradiated TiN (label B, dotted lines) and AlN (label D, dotted lines) layers. Light gray curves are reference spectra [17]. Adapted with permission from Surf. Sci. Spectra **21,** 35 (2014).

Mainly four chemically distinctive regions appear in the chemical images; they have been labeled on the Ti picture as A, B, C and D corresponding to non-irradiated and irradiated TiN, and AlN, respectively. Ti $2p_{3/2}$, N 1s and Al 2p core level spectra have been acquired from these points and shown in Fig. 5(b). Below each core level we have reported additional spectra extracted from a well-suited literature spectra [17], shown as light gray curves, where the Ti-Al-N compounds at variable stoichiometries have been investigated by XPS. As will be discussed later such reference spectra might help us to perform the analysis of the concentrations on the new chemical phases induced by the ion-beam interaction (see Fig. 3). The Ti $2p_{3/2}$ and N 1s spectra acquired on the point-A have an almost identical spectral shape as the spectra of pure TiN phase. The main component in the Ti $2p_{3/2}$ spectrum is located at 455.1 eV binding energy, and its shake-up peaks at 457.5 eV; they are in good agreement with reported literature values [17-20]. It is possible that a minor amount of TiO_x and/or TiN_xO_y might be present on the sample since a tiny O 1s peak was detected in the survey spectra almost everywhere. The N 1s spectrum has a main component at 397.3 eV binding energy which is assigned to the TiN form [14-19] with a shoulder at lower binding energy, which can be attributed to N-C bonds in form of TiN_xC_y and/or disordered TiN structures [21-26]. Point-C, which corresponds to a pure AlN layer, shows accordingly only Al and N signals. The Al 2p core line is broader than the reference spectrum. Additional components, in fact, are visible at both higher and lower binding energies; they could be

attributed to the presence of additional aluminum oxide forms, and substoichiometric and non-ordered crystallographic AlN domains, respectively[21-23,27]. Similar considerations are valid also for the N 1s peaks having major contributions centered at 397.7 eV. The Ti $2p_{3/2}$ core levels recorded in point-B and D demonstrate the dramatic effects of ion irradiation. In the TiN layer a new lineshape of the Ti 2p slightly shifts to higher binding energies, and the shake-up peaks become more dominant in agreement with previously reported works [17,27]; a well spectral matching of the Ti 2p curve with reference spectrum [17] implies to a $Ti_{0.75}Al_{0.25}N$ ternary compound estimation. A significant Ti signal appears also in the AlN area at point-D where before irradiation it was absent, and the core level shape matches the $Ti_{0.65}Al_{0.35}N$ ternary compound. As expected the Al 2p spectrum of the AlN layer (point-D) shows a shift toward lower binding energies matching the energy position. It should be highlighted how the width of the peak decreases with respect to the non-irradiated region suggesting a sort of homogenization of the chemical structure which is also proven by the analysis of the transmission electron microscopy (TEM) images and selected area electron diffraction (SEAD) patterns reported in the next section.

Cross-sectional TEM analysis revealed that ion irradiation strongly affects the structure, up to the depth of the Ar ion range, which covers approximately top 8 AlN/TiN bilayers (~140 nm). In the deeper region beyond the Ar ion range, the multilayered structure remains unaltered. This proves that the observed modifications result only from ion-beam interaction with the target material, without any side effects, such as beam heating of the target during ion irradiation. Hence, the applied high dose argon ion irradiation enabled the intermixing of the investigated AlN(8 nm)/TiN(9.3 nm) multilayers at room temperature, although these structures are thermodynamically stable up to 1000 ^{o}C. Such behavior was discussed previously [8,9,13], and can be assigned to a large number of knocked-on atoms that cross over the multiple interfaces in this very thin layer arrangement, already in the initial ballistic regime of ion-beam mixing [28]. The large amount of knock-ons could not be compensated by the repelling effect of chemical driving forces in this immiscible system.

Bright-field cross-sectional TEM images showing the top regions of non-irradiated and irradiated samples are presented in Fig. 6(a,b). Insets in the figures are the corresponding SAED patterns. TEM image of non-irradiated sample exhibits well separated individual layers, where bright contrast represents AlN and dark contrast TiN layers. Diffraction rings in the SAED pattern taken from this sample identify isolated hcp AlN and fcc TiN phases, with very fine nanocrystalline grains. Scattered bright spots appearing in the pattern represent reflections arising from the single crystal Si-substrate. The irradiated sample still exhibits some form of a layered structure, but the layers become thicker and

the contrast appears rather uniform, indicating that initially isolated phases become intermixed. A closer analysis shows that TiN layers appear to grow in thickness, consuming the adjacent AlN layers. It is also observed that individual crystal grains grow much larger upon ion irradiation. SAED pattern in this case corresponds to a dominant fcc phase, with some weak reflections from the remaining hcp AlN. Diffraction rings become sharper due to larger grains, the circles appearing as continued dotted lines.

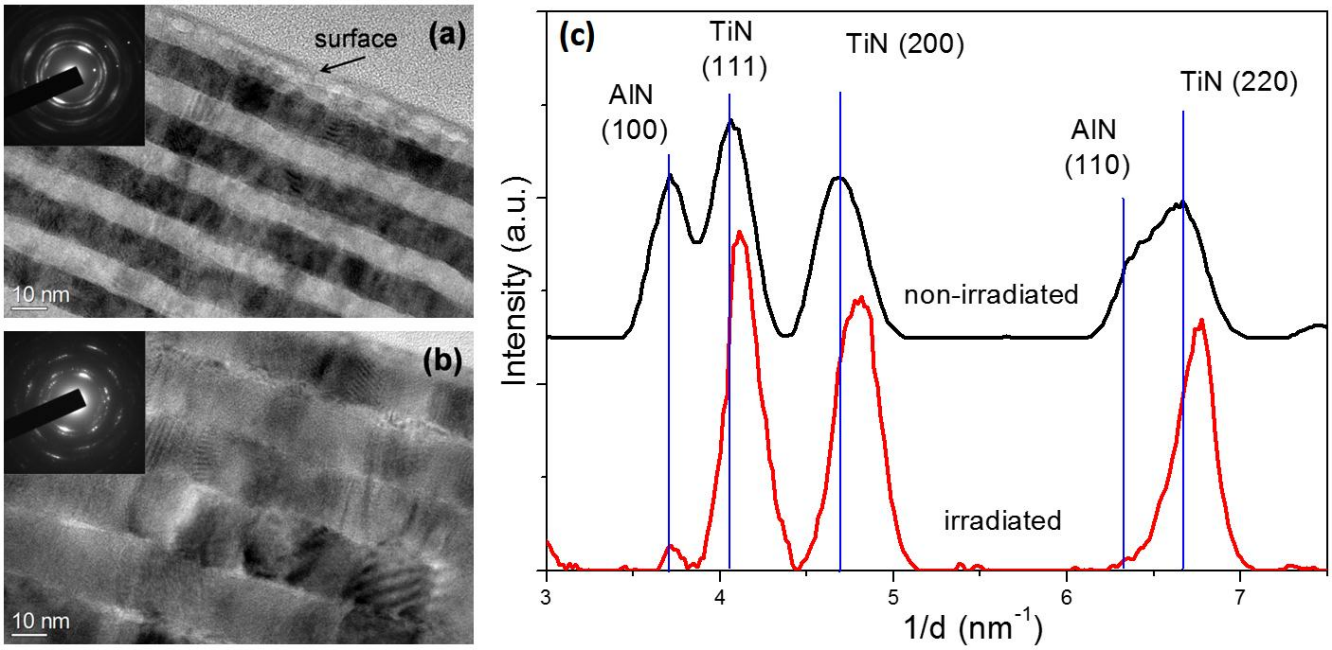

Fig 6. Cross-sectional TEM analysis of non-irradiated (a) and irradiated (b) samples and (c) extracted diffraction ring intensities from SAED patterns taken from non-irradiated and irradiated samples.

In order to compare the SAED patterns from Fig.6(a,b), extracted intensities of the diffraction rings are plotted in Fig. 6c. It can be seen that the main peaks corresponding to fcc TiN phase in the non-irradiated sample shift by 1-2% to lower crystal interplanar spacing, d, in the irradiated sample. This indicates a phase transformation from TiN to Al deficient TiAlN phase. Such parameter shift from pure fcc TiN lattice to lower d values is typical for Al deficient ternary TiAlN compounds, and it depends on the amount of incorporated Al [29]. The detected phase transformation into TiAlN ternary compounds, the Al deficiency in the formed new structures with lower interplanar lattice spacing and higher structural homogeneity are in agreement with the SPEM findings.

5. Conclusion

The investigated AlN/TiN multilayered structure suffered thorough structural and compositional modifications upon the applied heavy dose argon ion irradiation at room temperature. The observed

modifications are restricted to the ion penetration depth, proving that they result only from ion beam interaction, without any side effects such as beam heating of the target. The results indicate a pronounced inter-layer mixing, atomic redistribution and phase transformation. Intense intermixing is assigned to a large amount of knocked-on atomic species that cross over the multiple interfaces in this very thin layer arrangement, already in the ballistic regime. In the modification processes the original TiN layers appear to grow in thickness and grain size, retaining the fcc crystalline structure, while the adjacent AlN layers become diluted in the mix. In-depth compositional studies reveal that these largely grown fcc crystalline grains consist of Al deficient $Ti_{0.75}Al_{0.25}N$ and $Ti_{0.65}Al_{0.35}N$ ternary compounds. The results can be interesting for further studies of the role of individual layer thickness and the effects of heavy ion irradiation on immiscible ceramic multilayered nanocomposites, towards the development of new radiation tolerant materials.

Acknowledgments

This work was supported the Serbian Ministry of Education, Science and Technological Development (project ON 171023), ERC Advanced Investigator grant (226470 SILAMPS), and the International Atomic Energy Agency, Vienna (CRP 12024). We thank Petro Parisse and Loredana Casalis of the NanoInnovation Laboratory of Elettra - Sincrotrone Trieste SCpA for the AFM measurements.

Reference

[1] R. W. Grimes, R. J. M. Konings, L. Edwards, Greater tolerance for nuclear materials, Nat. Mater. **7** (2008) 683 – 685. (http://doi.org/10.1038/nmat2266)

[2] A. Misra, M. J. Demkowicz, X. Zhang, R. G. Hoagland, The radiation damage tolerance of ultra-high strength nanolayered composites, JOM **59** (2007) 62 - 65. (http://doi.org/10.1007/s11837-007-0120-6)

[3] T. Höchbauer, A. Misra, K. Hattar, R. G. Hoagland, Influence of interfaces on the storage of ion-implanted He in multilayered metallic composites, J. Appl. Phys. **98(12)** (2005) 123516. (http://doi.org/10.1063/1.2149168)

[4] Y. Gao, T. Yang, J. Xue, S. Yan, S. Zhou, Y. Wang, D. T. K. Kwok, P. K. Chu, Y. Zhang, Radiation tolerance of Cu/W multilayered nanocomposites, J. Nucl. Mater., **413** (2011) 11 – 15. (http://doi.org/10.1016/j.jnucmat.2011.03.030)

[5] K. Y. Yu, Y. Liu, E. G. Fu, Y. Q. Wang, M. T. Myers, H. Wang, L. Shao, X. Zhang, Comparisons of radiation damage in He ion and proton irradiated immiscible Ag/Ni nanolayers, J. Nucl. Mater., **440** (2013) 310 – 318. (http://dx.doi.org/10.1016/j.jnucmat.2013.04.069)

[6] M. Milosavljević, V. Milinović, D. Peruško, A. Grce, M. Stojanović, D. Pjević, M. Mitrić, J. Kovač, K. P. Homewood, Stability of nano-scaled Ta/Ti multilayers upon argon ion irradiation, Nucl. Instr. Meth. Phys. Res. Sect. B **269** (2011) 2090 – 2097. (http://doi.org/10.1016/j.nimb.2011.06.017)

[7] I. J. Beyerlein, A. Caro, M. J. Demkowicz, N. A. Mara, A. Misra, B. P. Uberuaga, Radiation damage tolerant nanomaterials, Mater. Today **16** (2013) 443 – 449. (http://dx.doi.org/10.1016/j.mattod.2013.10.019)

[8] M. Milosavljević, D. Peruško, V. Milinović, Z. Stojanović, A. Zalar, J. Kovač, C. Jeynes, Ion irradiation stability of multilayered AlN/TiN nanocomposites, J. Phys. D: Appl. Phys. **43** (2010) 065302. (http://iopscience.iop.org/0022-3727/43/6/065302)

[9] M. Milosavljević, A. Grce, D. Peruško, M. Stojanović, J. Kovač, G. Dražič, A. Yu. Didyk, V. A. Skuratov, A comparison of Ar ion implantation and swift heavy Xe ion irradiation effects on immiscible AlN/TiN multilayered nanostructures, Mater. Chem. Phys. **133** (2012) 884 – 892. (http://doi.org/10.1016/j.matchemphys.2012.01.112)

[10] I. Kim, L. Jiao, F. Khatkhatay, M. S. Martin, J. Lee, L. Shao, X. Zhang, J. G. Swadener, Y. Q. Wang, J. Gan, J. I. Cole, H. Wang, Size-dependent radiation tolerance in ion irradiated TiN/AlN nanolayer films, J. Nucl. Mater. **441** (2013) 47 – 53. (http://dx.doi.org/10.1016/j.jnucmat.2013.05.035)

[11] M. Hong, F. Ren, H. Zhang, X. Xiao, B. Yang, C. Tian, D. Fu, Y. Wang, C, Jiang, Enhanced radiation tolerance in nitride multilayered nanofilms with small period-thicknesses, Appl. Phys. Lett. **101** (2012) 153117. (http://doi.org/10.1063/1.4759004)

[12] J. F. Ziegler, J. P. Biersack, U. Littmark, *The Stopping and Range of Ions in Solids* (Pergamon Press, New York, 1985), see www.srim.org.

[13] M. Milosavljević, M. Obradović, A. Grce, D. Peruško, D. Pjević, J. Kovač, G. Dražič, C. Jeynes, High dose ion irradiation effects on immiscible AlN/TiN nano-scaled multilayers, Thin Solid Films **544** (2013) 562 – 566. (http://dx.doi.org/10.1016/j.tsf.2012.12.068)

[14] L. Gregoratti, A. Barinov, E. Benfatto, G. Cautero, C. Fava, P. Lacovig, D. Lonza, M. Kiskinova, R. Tommasini, S. Mähl, W. Heichler, 48-Channel electron detector for photoemission spectroscopy and microscopy, Rev. Sci. Instrum. **75** (2004) 64. (http://doi.org/10.1063/1.1630837)

[15] C.J. Powell, A. Jablonski, Surface sensitivity of X-ray photoelectron spectroscopy, Nucl. Instr. Meth. Phys. Res. **601** (2009) 54 – 65. (http://doi.org/10.1016/j.nima.2008.12.103)

[16] Calidris-EM, Programs for Electron Crystallography, Sollentuna, Sweden, 2013, see www.calidris-em.com

[17] G. Greczynski, J. Jensen, J. E. Greene, I. Petrov, L. Hultman, X-ray Photoelectron Spectroscopy Analyses of the Electronic Structure of Polycrystalline $Ti_{1-x}Al_xN$ Thin Films with $0 \leq x \leq 0.96$, Surf. Sci. Spectra **21** (2014) 35 – 49. (http://doi.org/10.1116/11.20140506)

[18] D. Jaeger, J. Patscheider, Single Crystalline Oxygen-free Titanium Nitride by XPS, Surf. Sci. Spectra **20** (2013) 1. (http://doi.org/10.1116/11.20121107)

[19] C. Papp, G. Conti, B. Balke, S. Ueda, Y. Yamashita, H. Yoshikawa, Y. S. Uritsky, K. Kobayashi, C. S. Fadley, Nondestructive characterization of a TiN metal gate: Chemical and structural properties by means of standing-wave hard x-ray photoemission spectroscopy, J. Appl. Phys. **112** (2012) 114501. (http://doi.org/10.1063/1.4765720)

[20] D. A. Jaeger, Ph.D. thesis, École polytechnique fédérale de Lausanne, Lausanne, 2012.

[21] G. Greczynski, I., Petrov, J. Greene, L. Hultman, Al capping layers for nondestructive x-ray photoelectron spectroscopy analyses of transition-metal nitride thin films, J. Vac. Sci. Technol. A **33** (2015) 05E101. (http://doi.org/10.1116/1.4916239)

[22] R. Ananthakumar, B. Subramanian, A. Kobayashi, M. Jayachandran, Electrochemical corrosion and materials properties of reactively sputtered TiN/TiAlN multilayer coatings, Ceram. Int. **38** (2012) 477 – 485. (http://doi.org/10.1016/j.ceramint.2011.07.030)

[23] L. Rosenberger, R. Baird, E. McCullen, G. Auner, G. Shreve, XPS analysis of aluminum nitride films deposited by plasma source molecular beam epitaxy, Surf. Interface Anal. **40** (2008) 1254 – 1261. (http://doi.org/10.1002/sia.2874)

[24] J. Marco, J. Gancedo, M. Auger, O. Sánchez, J. M. Albella, Chemical stability of TiN, TiAlN and AlN layers in aggressive SO2 environments, Surf. Interface Anal. **37** (2005) 1082 – 1091. (DOI: 10.1002/sia.2083)

[25] A. Agudelo, J. Gancedo, J. Marco, D. Hanzel, Corrosion resistance of titanium nitride and mixed titanium/titanium nitride coatings on iron in humid SO_2-containing atmospheres, J. Vac. Sci. Technol. A **15** (1997) 3163. (http://doi.org/10.1116/1.580862)

[26] P.-Y. Jouan, M.-C. Peignon, C. Cardinaud, G. Lemperiere, Characterisation of TiN coatings and of the TiN/Si interface by X-ray photoelectron spectroscopy and Auger electron spectroscopy, Appl. Surf. Sci. **68** (1993) 595 – 603. (http://dx.doi.org/10.1016/0169-4332(93)90241-3)

[27] P. Shum, Z. Zhou, K. Li, Y. Shen, XPS, AFM and nanoindentation studies of $Ti_{1-x}Al_xN$ films synthesized by reactive unbalanced magnetron sputtering, Mater. Sci. Eng., B **100** (2003) 204 – 203. (http://dx.doi.org/10.1016/S0921-5107(03)00107-7)

[28] B. X. Liu, W. S. Lai, Q. Zhang, Irradiation induced amorphization in metallic multilayers and calculation of glass-forming ability from atomistic potential in the binary metal systems, Mater. Sci. Eng. R. **29** (2000) 1 – 48. (http://dx.doi.org/10.1016/S0927-796X(00)00016-4)

[29] M. Arndt, T. Kacsich, Performance of new AlTiN coatings in dry and high speed cutting, Surf. Coat. Technol. **163-164** (2003) 674 - 680. (http://dx.doi.org/10.1016/S0257-8972(02)00694-1)